Eur. Phys. J. C (2017) 77:794
https://doi.org/10.1140/epjc/s10052-017-5354-z

THE EUROPEAN PHYSICAL JOURNAL C



Regular Article - Theoretical Physics

# Extracting the top-quark running mass using $t\bar{t}$ + 1-jet events produced at the Large Hadron Collider

**J. Fuster**[1], **A. Irles**[2,3,a], **D. Melini**[1,4], **P. Uwer**[5], **M. Vos**[1]

[1] IFIC, Universitat de València and CSIC, Catedrático Jose Beltrán 2, 46980 Paterna, Spain
[2] Laboratoire de l'Accélérateur Linéaire, Centre Scientifique d'Orsay, Université de Paris-Sud XI, CNRS/IN2P3, 91898 Orsay Cedex, France
[3] Deutsches Elektronen-Synchrotron (DESY), Notkestraße 85, 22607 Hamburg, Germany
[4] Departamento de Fisica Teórica y del Cosmos, Universidad de Granada, Campus Fuentenueva, 18071 Granada, Spain
[5] Humboldt-Universität zu Berlin, Newtonstrasse 15, 12489 Berlin, Germany

Received: 7 April 2017 / Accepted: 5 November 2017


**Abstract** We present the calculation of the next-to-leading order QCD corrections for top-quark pair production in association with an additional jet at hadron colliders, using the modified minimal subtraction scheme to renormalize the top-quark mass. The results are compared to measurements at the Large Hadron Collider run I. In particular, we determine the top-quark running mass from a fit of the theoretical results presented here to the LHC data.

## 1 Introduction

The top quark is the heaviest elementary particle discovered so far. More than 25 years after its discovery at Fermilab [1,2] a detailed understanding of why the top quark is so heavy is still lacking. With a mass of

$$m_t = 173.34 \pm 0.27\ (\text{stat.}) \pm 0.71\ (\text{syst.})\ \text{GeV}\ [3] \qquad (1)$$

the top quark is roughly as heavy as a gold atom and more than 30 times heavier than the next comparable heavy quark, the bottom quark. While the top-quark mass may seem unnaturally large compared to the lighter quark masses it appears rather natural given the size of the top-quark Yukawa coupling which is approximately one. Within the Standard Model (SM) of particle physics, the top-quark mass is an important input parameter influencing a variety of theoretical predictions:

1. In the SM the W-boson mass, the Higgs boson mass and the top-quark mass are related. A precise measurement of the three masses thus gives an important test of the SM.
2. The vacuum stability, analyzed through the behavior of the Higgs boson effective potential, is very sensitive to the top-quark mass. Given the current measurements, recent analysis shows that the vacuum is most likely metastable – with a lifetime, however, larger than the age of the universe [4,5].
3. Despite the large mass gap between the top-quark mass and the bottom-quark mass, the top quark highly influences the properties of B hadrons.

While not being exhaustive the aforementioned examples nicely illustrate the importance of precise determinations of the top-quark mass. Tremendous efforts have been made in the past to improve existing methods and to develop new approaches. For an overview we refer to Refs. [6,7]. Because of its short lifetime the top quark is not observed as a free particle. As a consequence, all top-quark mass determinations rely to some extent on indirect determinations: the mass value is inferred by comparing the measurements with theoretical predictions depending on the top-quark mass. Obviously, the accuracy of the procedure depends on the quality of the measurements as well as on the uncertainties of the theoretical predictions. Since QCD corrections can easily lead to corrections of the order of ten per cent, at least next-to-leading order (NLO) corrections should be taken into account. Including radiative corrections allows one also to give a unique interpretation of the determined mass value within a specific renormalization scheme. In particular, this gives the opportunity to consider other renormalization schemes than the usually adopted pole mass scheme. In fact, the mass quoted in Eq. (1) does not correspond to a well-defined renormalization scheme. Very often this mass is identified as the so-called Monte Carlo mass, since template fits and kinematical reconstruction use Monte Carlo predictions to determine the mass value. Although a rigorous proof is lacking it is often assumed

[a] e-mail: irles@lal.in2p3.fr

Published online: 22 November 2017

that the mass value is very close to the pole mass. Using alternative methods in which the renormalization scheme is better controlled thus may provide valuable cross checks. In addition, different schemes may show different behavior within perturbation theory. The freedom to choose the scheme can thus be exploited to improve the mass determination in specific cases. For example, it is well known that the threshold behavior of top-quark pair production in electron–positron annihilation is badly described within perturbation theory when the top-quark pole mass is used (see for example Ref. [8] and the references therein). It is also well known that the pole mass concept suffers from the so-called renormalon ambiguity reflecting the fact that the pole mass is strictly speaking not well defined in QCD because of confinement [9,10]. While the related uncertainty of order $\Lambda_{\mathrm{QCD}}$[1] might still be negligible in view of the precision reached in current measurements, it is nevertheless highly interesting and well motivated to investigate also top-quark mass measurements using alternative mass definitions. This has been done for the first time in Ref. [12] where the determination of the top-quark mass in the modified minimal subtraction/running mass scheme ($\overline{\mathrm{MS}}$) has been studied. The analysis is based on cross section measurements at the Tevatron. Using in the theoretical predictions the $\overline{\mathrm{MS}}$ mass instead of the pole mass, the comparison with the experimentally measured cross sections gives direct access to the running mass. The results obtained in Ref. [12] and subsequent determinations are consistent with the pole mass measurements. Similar studies have been performed at the LHC. Very recently, the analysis has been extended to single top-quark production [13].

In Ref. [14] an alternative observable to determine the top-quark mass has been proposed. In this case, top-quark pairs in association with an additional jet are considered instead of the inclusive cross section for top-quark pair production. Since the emission of an additional jet also depends on the top-quark mass, this process has a high sensitivity to the mass parameter. Indeed, it has been shown in Ref. [14] that the invariant mass distribution of the $t\bar{t}$–jet system significantly enhances the mass effects. In Refs. [15,16] the method has been employed to determine the top-quark pole mass using LHC run I data. The aim of this article is to extend the calculation of Ref. [14] to the $\overline{\mathrm{MS}}$ scheme and apply the method to extract the running mass $m_t(m_t)$ using published results from the ATLAS experiment [15]. This may serve as a proof of concept as well as a consistency check of the existing measurement. The article is organized as follows. In Sect. 2 theoretical results using the running top-quark mass are presented. Using these results we determine in Sect. 3 the running top-quark mass from a comparison with published experimental results [15]. We finally close with a short conclusion in Sect. 4.

[1] Recent work indicates that the uncertainty is below 100 MeV [11].

## 2 Theoretical predictions using the $\overline{\mathrm{MS}}$ mass

We study the process

$$pp \to t\bar{t} + 1\text{-jet} + X. \tag{2}$$

Note that a minimal $p_T$ of the additional jet is required to separate the process from inclusive top-quark pair production and render the cross section infrared finite. In the following, we adopt the 50 GeV cut also applied in the experimental analysis [15]. The NLO corrections for top-quark pair production in association with an additional jet have been calculated first in Refs. [17,18] and later in Refs. [19,20]. In Refs. [17,18] as well as in Refs. [19,20] the top-quark mass is renormalized in the pole mass scheme. In the pole mass scheme the top-quark mass $M_t^{\mathrm{pole}}$ is defined as the location of the pole of the perturbatively calculable top-quark propagator. In Refs. [17,18] it has been shown that the QCD corrections, although not negligible, are moderate in size. In particular, the scale dependence is stabilized in NLO and shows a plateau at $\mu_r = M_t^{\mathrm{pole}}$ where $\mu_r$ denotes the renormalization scale which is set equal to the factorization scale $\mu_f$. In Ref. [14] these findings have been extended by the observation that also different approximations in the theoretical description (fixed order, $t\bar{t}+X$ + parton shower, $t\bar{t}+1$-jet$+X$ + parton shower), using again the top-quark pole mass, show remarkably consistent results. Given the stability with respect to radiative corrections, it has been argued in Ref. [14] that top-quark pair production in association with an additional jet may provide a promising alternative to measure the top-quark mass. As an observable the quantity

$$\mathcal{R}(M_t^{\mathrm{pole}}, \rho_s) = \frac{1}{\sigma_{t\bar{t}+1\text{-jet}}} \frac{\mathrm{d}\sigma_{t\bar{t}+1\text{-jet}}}{\mathrm{d}\rho_s}(M_t^{\mathrm{pole}}, \rho_s) \tag{3}$$

has been proposed. Here $\sigma_{t\bar{t}+1\text{-jet}}$ is the total cross section for $pp \to t\bar{t}$ + 1-jet (including the $p_T$ cut) and $\rho_s$ is a dimensionless variable defined as

$$\rho_s = \frac{2m_0}{\sqrt{s_{t\bar{t}j}}}, \tag{4}$$

where $m_0$ is an 'arbitrary' mass scale of the order of the top-quark mass. In the following $m_0 = 170$ GeV is used. The distribution $\mathcal{R}(M_t^{\mathrm{pole}}, \rho_s)$ has been successfully used by the LHC experiments ATLAS and CMS to determine the top-quark mass in the pole mass scheme [15,16]. Since the aim of this article is to repeat the analysis using, however, the mass parameter renormalized in the $\overline{\mathrm{MS}}$ scheme, theoretical predictions within this scheme are required. Owing to the Lehmann–Symanzik–Zimmermann formalism an ab initio calculation using the $\overline{\mathrm{MS}}$ scheme is non-trivial. To obtain results in the $\overline{\mathrm{MS}}$ scheme we thus follow the method developed in Ref. [12]. To illustrate the main idea and for conve-

nience, we briefly outline the approach for the cross section. The same technique is also applicable to each individual bin of a differential distribution. The relation between the $\overline{\text{MS}}$ mass $m_t(\mu)$ and the pole mass $M_t^{\text{pole}}$ is given by

$$M_t^{\text{pole}} = m_t(\mu)\left(1+\hat{a}(\mu)\frac{4}{3}\left[1-\frac{3}{4}\ln\left(\frac{m_t^2}{\mu^2}\right)\right]\right)+O(\hat{a}^2) \tag{5}$$

with

$$\hat{a}(\mu) = \frac{\alpha_s^{(6)}(\mu)}{\pi} \tag{6}$$

where $\alpha_s^{(6)}(\mu)$ is the QCD coupling constant of the strong interaction in the six flavor theory. In Refs. [17,18] the closed top-quark loop has been subtracted at finite momentum. At the order we are working here the coupling constant defined in this way corresponds to the coupling constant in the five flavor theory. Since the difference between $\alpha_s^{(5)}(\mu)$ and $\alpha_s^{(6)}(\mu)$ is again a higher-order effect we can replace in Eq. (5) $\hat{a}(\mu)$ by

$$a(\mu) = \frac{\alpha_s^{(5)}(\mu)}{\pi} \tag{7}$$

to obtain

$$M_t^{\text{pole}} = m_t(m_t)\left(1+a(\mu)\frac{4}{3}\right)+O(a^2). \tag{8}$$

Note that we have replaced $a(m_t)$ by $a(\mu)$, which is again a higher-order effect. In the pole mass scheme the expansion of the cross section $\sigma$ reads

$$\sigma = a(\mu)^3\sigma^{(0)}(M_t^{\text{pole}}) + a(\mu)^4\sigma^{(1)}(M_t^{\text{pole}}) + \cdots, \tag{9}$$

where $\sigma^{(0)}$, $\sigma^{(1)}$ denote the expansion coefficients. For simplicity, we have suppressed all further dependence of $\sigma^{(0)}$ and $\sigma^{(1)}$. Using the relation between the pole mass and the $\overline{\text{MS}}$ mass given above we get

$$\sigma = a(\mu)^3\sigma^{(0)}\left(m_t(m_t)(1+\frac{4}{3}a(\mu)+\cdots)\right) + a(\mu)^4\sigma^{(1)}\left(m_t(m_t)(1+\frac{4}{3}a(\mu)+\cdots)\right)+\cdots \tag{10}$$

Working in fixed-order perturbation theory we have to expand in the coupling constant:

$$\sigma = a(\mu)^3\sigma^{(0)}(m_t(m_t)) + a(\mu)^4\left[\sigma^{(1)}(m_t(m_t)) + \frac{4}{3}m_t(m_t)\left.\frac{\mathrm{d}\sigma^{(0)}(M_t^{\text{pole}})}{\mathrm{d}M_t^{\text{pole}}}\right|_{M_t^{\text{pole}}=m_t(m_t)}\right]+O(a^5). \tag{11}$$

The two contributions $\sigma^{(0)}(m_t(m_t))$ and $\sigma^{(1)}(m_t(m_t))$ are trivial to compute: one just evaluates the corresponding cross sections with the pole mass set to the numerical value of $m_t(m_t)$. The third term is a bit more cumbersome. Instead of evaluating the derivative analytically, we decided to compute it numerically. To do so we computed $\sigma^{(0)}(m_t(m_t)\pm\Delta)$ and $\sigma^{(0)}(m_t(m_t)\pm 2\Delta)$ and used

$$\frac{\mathrm{d}f(x)}{\mathrm{d}x} = \frac{f(x+\Delta)-f(x-\Delta)}{2\Delta}+O(\Delta^2) \tag{12}$$

as well as

$$\frac{\mathrm{d}f(x)}{\mathrm{d}x} = \frac{1}{12\Delta}\Big(f(x-2\Delta)-8f(x-\Delta) +8f(x+\Delta)-f(x+2\Delta)\Big)+O(\Delta^4). \tag{13}$$

As a further consistency check, we used different values for $\Delta$: 1, 0.5 and 0.25 GeV. Using different discretizations and different approximations lead to differences for the cross section at the per mille level.

When applying this method to the $t\bar{t}$ + 1-jet + $X$ cross section at 7 TeV as a function of the $\overline{\text{MS}}$ mass $m_t(m_t)$ we obtain the results shown in Fig. 1. As in Refs. [14,15] the jets are defined using the anti-kt algorithm [21] as implemented in the FastJet package [22] with $R = 0.4$ and a recombination according to the $E$-scheme. Furthermore, as stated above the additional jet is required to have $p_T > 50$ GeV and in accordance with Ref. [15] $|\eta| < 2.5$ where $\eta$ defines the pseudo-rapidity. As far as the coordinate system is concerned,

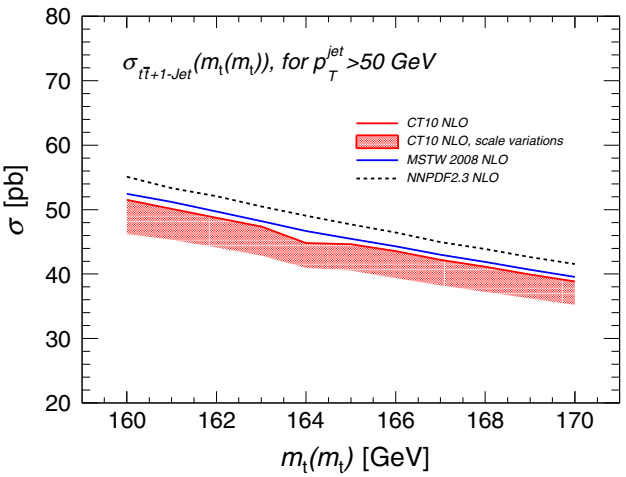


**Fig. 1** The $t\bar{t}$ + 1-jet + $X$ cross section at NLO QCD for proton-proton collisions at 7 TeV as a function of the running mass $m_t(m_t)$. The lines show the result of the calculation for $\mu = m_t(m_t)$ using different PDF sets: CT10 NLO (red solid line), MSTW2008nlo90cl (blue dashed-dotted line), NNPDF2.3 NLO PDF (black dashed line). The red shaded area shows the impact of the scale variation for the CT10 NLO PDF set, where $\mu = \mu_r = \mu_f$ has been varied in the range $m_t(m_t)/2 \le \mu \le 2m_t(m_t)$

we follow the LHC convention which defines the $z$-direction along the beam axis and the origin as the nominal interaction point. For more details we refer to Ref. [15] (footnote below Eq. (2)). Having applied the same cuts as in Ref. [15] the results for $\mathcal{R}$ presented here may be directly compared with the unfolded results as presented in Ref. [15].

To study the PDF dependence of the theoretical predictions, three different PDF sets are employed: the CT10 NLO PDF set [23], which is the nominal PDF set used for the top-quark pole mass extraction in Ref. [15], the MSTW2008nlo90cl PDF set [24], and the NNPDF2.3 NLO PDF set [25]. The MSTW2008 NLO and the NNPDF2.3 NLO sets are chosen to follow as closely as possible the analysis performed in Ref. [15] where the two sets have been used to estimate the PDF effects. CT10 NLO and MSTW2008 give rather consistent results, deviating in most cases less than two per cent from each other. The NNPDF2.3 NLO PDF leads to larger results which differ by about four per cent from MSTW2008. Given the progress concerning the PDF determinations recent PDF sets should show for even smaller differences.

To estimate the effect of higher-order corrections we calculate for the CT10 NLO PDF set the impact of the scale dependence varying the scale as usual by a factor 2 up and down around the central scale set to $\mu = m_t(m_t)$. Similar to what has been observed in Refs. [17,18] when using the pole mass, the predictions for the cross section for $\mu = 2m_t(m_t)$ and $\mu = 0.5m_t(m_t)$ are both smaller than the result for $\mu = m_t(m_t)$, showing a plateau around $\mu = m_t(m_t)$. The band in Fig. 1 shows the largest variation with respect to the nominal value for $\mu = m_t(m_t)$. With respect to the central value of the band, the scale uncertainty amounts to an effect of about $\pm 5\%$ – slightly smaller than the scale uncertainty observed using the pole mass definition. This is very similar to what is observed for the inclusive top-quark pair production cross section. Note that this is merely a kinematic effect as in the $\overline{\text{MS}}$ scheme the leading-order results increase because of the numerically smaller mass value. The NLO corrections decrease accordingly and thus lead to a smaller scale dependence.

To calculate the $\mathcal{R}$ distribution defined in Eq. (3) using the $\overline{\text{MS}}$ mass, we apply the same strategy as for the cross section employing, however only the two-point formulas of Eq. (12) together with a step size of $\Delta = 0.5$ GeV. For one mass value we cross checked the procedure using the five point formulas with a step size of 0.25 GeV. We found consistent results at the per mille level. The results for $\mathcal{R}$ for the different bins in $\rho_s$ are shown in Figs. 2 and 3. The definition of the bin boundaries follows the setup used in Refs. [15]. Again the calculation has been done for three different scales $\mu = m_t(m_t)/2, m_t(m_t), 2m_t(m_t)$. The predictions for $\mathcal{R}$ for different values of $m_t(m_t)$ are given in Table 1. The upper and lower subscripts denote the shift with respect to the central scale $\mu = m_t(m_t)$ (the upper value gives the shift for $\mu = 2m_t(m_t)$, the lower value gives the shift for $\mu = m_t(m_t)/2$). As for the $t\bar{t}$ + 1-jet cross section

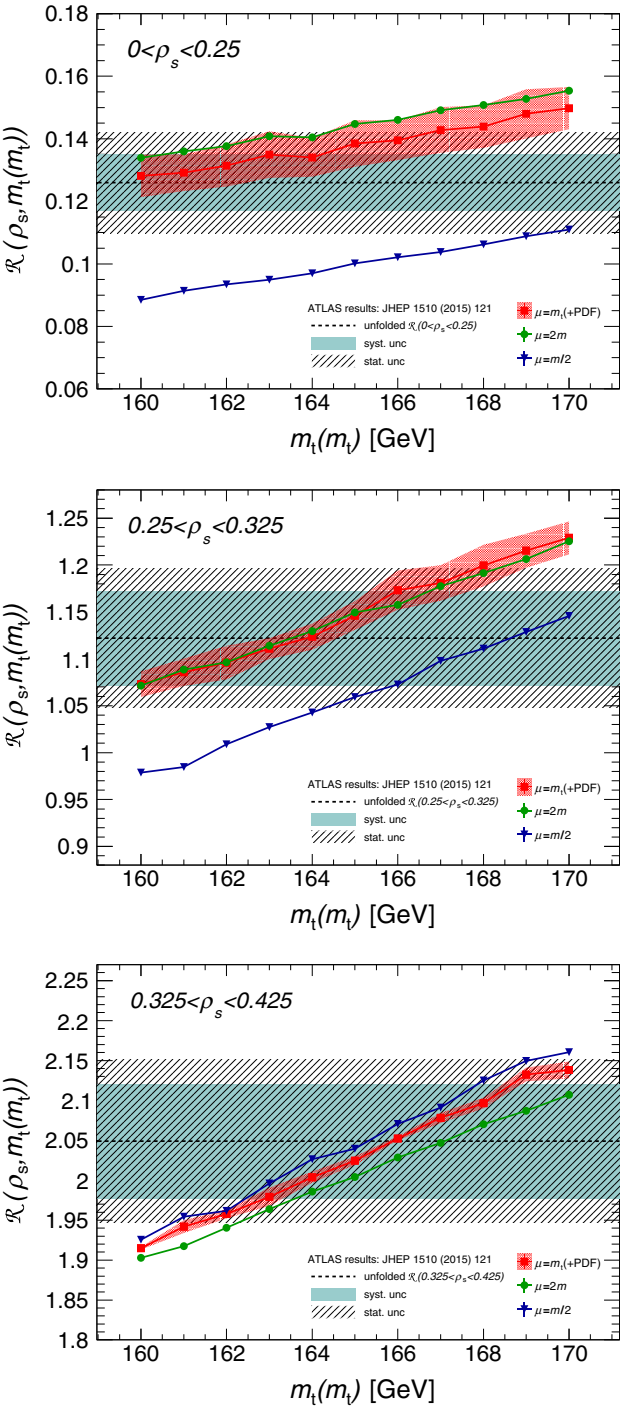


**Fig. 2** $\mathcal{R}$ as defined in Eq. (3) as a function of $m_t(m_t)$ for the $\rho_s < 0.425$ intervals using the CT10 PDF set. The red squares show the results for the central scale $\mu = \mu_r = \mu_f = m_t(m_t)$. The red band illustrates the impact of using the MSTW2008 or the NNPDF2.3 PDF set. The blue triangles (green dots) show the results for $\mu = m_t(m_t)/2$ ($\mu = 2m_t(m_t)$). For comparison we also illustrated as dashed line the measured result as reported in Ref. [15]. The bands show the systematic and statistical uncertainty

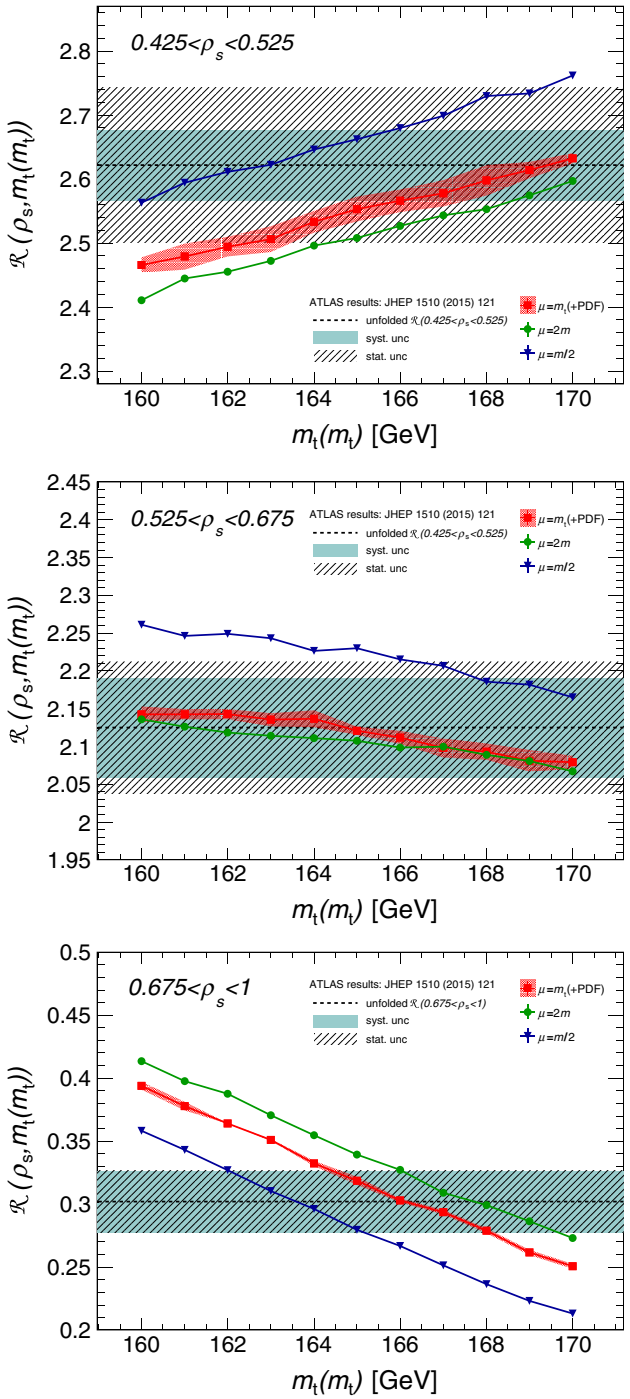


**Fig. 3** Same as Fig. 2 but for the $\rho_s > 0.425$ intervals

we employ the CT10 PDF set. Results for the two other PDF sets used in this analysis are given in the appendix in Table 3 for the NNPDF PDF set and Table 4 for the MSTW PDF set. In Figs. 2 and 3 the red squares show the results for the central scale, while the blue triangles (green circles) show the results for $\mu = m_t(m_t)/2$ ($\mu = 2m_t(m_t)$). To illustrate the PDF dependence, the dotted band shows the maximal shift of

**Table 1** The $\mathcal{R}(m_t(m_t))$-distribution calculated using $t\bar{t}$ + 1-jet samples at NLO accuracy for different $m_t(m_t)$ values for the CT10 PDF set. The predictions for $\mu = m_t$ are quoted as central values. The shifts correspond to the difference $(\mathcal{R}(m_t, \mu = x) - \mathcal{R}(m_t, \mu = m_t))$ where the results for $x = 2m_t$ and $x = m_t/2$ are quoted as upper-scripts and lower-scripts correspondingly

| Bin, range in $\rho_s$ | $\mathcal{R}(m_t(m_t))$ | | |
|---|---|---|---|
| | 160 GeV | 161 GeV | 162 GeV |
| 1, 0–0.25 | $0.128^{+0.006}_{-0.040}$ | $0.129^{+0.007}_{-0.038}$ | $0.131^{+0.006}_{-0.038}$ |
| 2, 0.25–0.325 | $1.073^{-0.001}_{-0.094}$ | $1.086^{+0.003}_{-0.101}$ | $1.096^{+0.000}_{-0.087}$ |
| 3, 0.325–0.425 | $1.915^{-0.012}_{+0.011}$ | $1.942^{-0.024}_{+0.012}$ | $1.957^{-0.017}_{+0.004}$ |
| 4, 0.425–0.525 | $2.466^{-0.055}_{+0.097}$ | $2.479^{-0.034}_{+0.115}$ | $2.495^{-0.039}_{+0.117}$ |
| 5, 0.525–0.675 | $2.142^{-0.006}_{+0.119}$ | $2.143^{-0.016}_{+0.104}$ | $2.143^{-0.024}_{+0.106}$ |
| 6, 0.675–1.0 | $0.394^{+0.020}_{-0.036}$ | $0.378^{+0.020}_{-0.035}$ | $0.364^{+0.024}_{-0.037}$ |
| Bin | 163 GeV | 164 GeV | 165 GeV | 166 GeV |
| 1 | $0.135^{+0.006}_{-0.040}$ | $0.134^{+0.006}_{-0.037}$ | $0.139^{+0.006}_{-0.038}$ | $0.140^{+0.007}_{-0.037}$ |
| 2 | $1.111^{+0.003}_{-0.084}$ | $1.124^{+0.006}_{-0.081}$ | $1.146^{+0.003}_{-0.087}$ | $1.173^{-0.016}_{-0.101}$ |
| 3 | $1.979^{-0.015}_{+0.017}$ | $2.004^{-0.018}_{+0.023}$ | $2.024^{-0.020}_{+0.015}$ | $2.052^{-0.024}_{+0.018}$ |
| 4 | $2.506^{-0.034}_{+0.116}$ | $2.533^{-0.037}_{+0.113}$ | $2.553^{-0.045}_{+0.109}$ | $2.566^{-0.039}_{+0.114}$ |
| 5 | $2.135^{-0.021}_{+0.108}$ | $2.137^{-0.026}_{+0.090}$ | $2.121^{-0.013}_{+0.109}$ | $2.112^{-0.013}_{+0.103}$ |
| 6 | $0.351^{+0.020}_{-0.040}$ | $0.332^{+0.022}_{-0.036}$ | $0.319^{+0.021}_{-0.039}$ | $0.303^{+0.024}_{-0.036}$ |
| Bin | 167 GeV | 168 GeV | 169 GeV | 170 GeV |
| 1 | $0.143^{+0.006}_{-0.039}$ | $0.144^{+0.007}_{-0.038}$ | $0.148^{+0.005}_{-0.039}$ | $0.150^{+0.006}_{-0.039}$ |
| 2 | $1.181^{-0.003}_{-0.083}$ | $1.199^{-0.008}_{-0.089}$ | $1.215^{-0.009}_{-0.087}$ | $1.229^{-0.004}_{-0.083}$ |
| 3 | $2.078^{-0.031}_{+0.013}$ | $2.097^{-0.027}_{+0.028}$ | $2.132^{-0.045}_{+0.017}$ | $2.138^{-0.031}_{+0.022}$ |
| 4 | $2.578^{-0.034}_{+0.121}$ | $2.598^{-0.045}_{+0.132}$ | $2.614^{-0.040}_{+0.120}$ | $2.632^{-0.035}_{+0.130}$ |
| 5 | $2.098^{+0.002}_{+0.109}$ | $2.093^{-0.004}_{+0.092}$ | $2.081^{-0.000}_{+0.101}$ | $2.079^{-0.012}_{+0.086}$ |
| 6 | $0.294^{+0.015}_{-0.042}$ | $0.279^{+0.020}_{-0.042}$ | $0.262^{+0.025}_{-0.038}$ | $0.251^{+0.022}_{-0.037}$ |

the predictions with respect to the CT10 NLO PDF set using the MSTW2008nlo90cl and NNPDF2.3 NLO PDF sets. In addition to the theoretical predictions, we show as horizontal bands for each bin in $\rho_s$ the experimental result for $\mathcal{R}$ – unfolded to the parton level – as published in Table 4 of Ref. [15]. The dashed black line illustrates the central values, while the hashed band shows the statistical uncertainty and the solid band shows the systematic uncertainty. The systematic uncertainties include theoretical and experimental uncertainties. We stress that the results for $\mathcal{R}$ given in Table 4 of Ref. [15] have been unfolded to the parton-level, detector effects and hadronization effects are no longer accounted.

It is thus possible to directly compare the measurements with the theoretical predictions presented here. In particular, the theoretical results for $\mathcal{R}$ as a function of the top-quark $\overline{\text{MS}}$ mass, can be fitted to the unfolded distribution, leading to a determination of the top-quark mass in the $\overline{\text{MS}}$ scheme. Since the analysis presented in this paper relies on

the usage of unfolded data we may add some remarks concerning the unfolding. Although the full reconstruction of the top quarks is not required we stress that the reconstruction of the momenta of the final state objects which is required to determine the invariant mass squared $s_{t\bar{t}j}$, is highly non-trivial, since issues like missing energy, unobserved neutrinos, and combinatorial background have to be taken into account. In particular, the aforementioned issues will also lead to an additional uncertainty of the unfolding procedure. The unfolding performed in Ref. [15] is based on a modeling of various effects including estimates on the related uncertainties. Furthermore, it has been shown in Ref. [15] that the unfolding is, within the uncertainties, independent of the top-quark mass used in the unfolding procedure. Instead of performing the unfolding, a future mass determination could also employ more realistic theoretical predictions reducing or even avoiding the unfolding. As long as the uncertainties of the unfolding procedure are reliably estimated, we do not expect a major difference in the results, although the related uncertainties in the mass determination may be reduced using improved theoretical predictions. In particular, relying on a complete theoretical description of top-quark production and decay, including off-shell effects, using for example the recently published results on $e^+\nu_e\mu^-\bar{\nu}_\mu b\bar{b}j + X$ production [26,27] may reduce the theoretical uncertainties. As far as the combination with the parton shower is concerned, the recent developments on parton showers at NLO accuracy, taking into account intermediate resonances [28,29], may also help to further improve the theoretical predictions.

## 3 Proof of concept: determination of the top-quark running mass

In this section we use the theoretical results presented in the previous section to extract the top-quark $\overline{\text{MS}}$ mass from the experimental results published in Ref. [15].

As shown in Refs. [14,15], the most sensitive bin is the interval $0.675 < \rho_s < 1$. Very close to the kinematic threshold ($\rho_s \sim 1$), fixed-order calculations as presented in the previous section are most likely not sufficient, since bound-state effects and soft gluon emission may become important [30,31]. However, as has been shown in Refs. [30,31] the impact on the total cross section is small. As far as the $t\bar{t}$ invariant mass distribution is concerned a significant distortion due to (would-be) bound-state effects occurs only below or closely above the nominal threshold. In Ref. [15] the impact of the threshold region on the mass extraction has been investigated using different upper boundaries. As no significant variation of the extracted mass value was found, the range for the highest $\rho_s$-bin has been extended to 1 in Ref. [15]. We assume that the same holds true for the $\overline{\text{MS}}$ mass and use the same bin boundaries for the bin close to the threshold. This assumption is well justified given the current uncertainties.

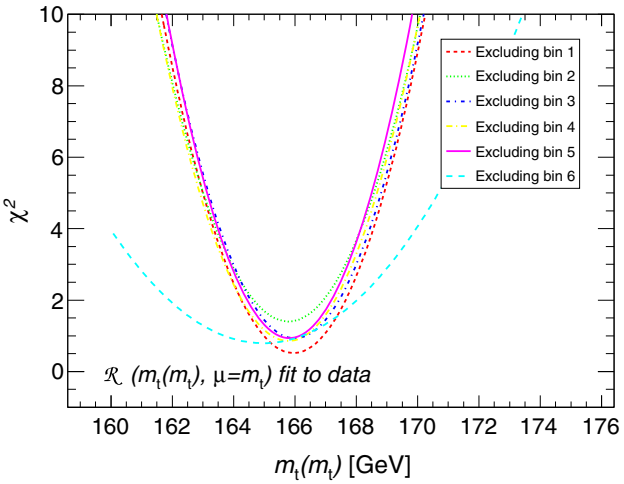


**Fig. 4** The $\chi^2$ as a function of $m_t(m_t)$ for different choices of the excluded bin. The bin boundaries for the six bins are given in Table 1

In complete analogy with what has been done in Ref. [15] we use a least-square fit and define the $\chi^2$ by

$$\chi^2 = \sum_{ij} \left[\mathcal{R}^{\text{corr.},i} - \mathcal{R}^i(m_t(m_t))\right] V_{ij}^{-1} \times \left[\mathcal{R}^{\text{corr.},j} - \mathcal{R}^j(m_t(m_t))\right], \quad (14)$$

where $\mathcal{R}^{\text{corr.},i}$ is the measured value in the $i$th bin – unfolded to the parton level – and $\mathcal{R}^i(m_t(m_t))$ denotes the theoretical prediction as a function of the running mass. Since the numerical evaluation of $\mathcal{R}^i(m_t(m_t))$ is very time consuming we calculate $\mathcal{R}^i(m_t(m_t))$ for $m_t(m_t)$ in the range 160–170 GeV in steps of one GeV and use a linear interpolation in between. The matrix $V^{-1}$ is the inverse of the statistical covariance matrix of the unfolded $\mathcal{R}$-distribution as given in Ref. [15] (Figure 8 provided as auxiliary material to Ref. [15]). The top-quark mass value is determined through a minimization of the $\chi^2$. We use only five of the six available bins because the number of degrees of freedom is reduced by one through the normalization of the $\mathcal{R}$ distribution. Figure 4 shows the results for different choices of the excluded bin. As long as the bin closest to the threshold is kept, very similar results are obtained. Excluding the highest bin, however, leads to an important change of the observed $\chi^2$. This is a direct consequence of the high sensitivity of the cross section in this bin to the top-quark mass together with the small experimental uncertainty of the measured value for this bin. The exclusion of the highest bin leads to a shift of about 1 GeV as far as the minimum of the $\chi^2$ is concerned. In addition, the minimum becomes significantly broader, reflecting the loss in sensitivity. For the extraction of the top-quark mass we follow the approach used in Ref. [15] and exclude the lowest bin which

corresponds to the most energetic events and has only a very weak sensitivity to the top-quark mass. The statistical uncertainty is taken as the mass shift that increases $\chi^2$ by one unit with respect to the minimum ($\Delta\chi^2 = +1$).

As the published results of Ref. [15] do not provide a full covariance matrix, including the breakdown of the systematic uncertainties, we use a modified version of the $\chi^2$ function where no covariance matrix is assumed to evaluate the systematic uncertainties:

$$\chi^2 = \sum_i \frac{\left[\mathcal{R}^{\text{corr.},i} - \mathcal{R}^i(m_t(m_t))\right]^2}{\mathcal{R}^i(m_t(m_t))}. \quad (15)$$

The fit is repeated 5000 times with pseudo data varying the value of $\mathcal{R}^{\text{corr.},i}$ assuming a gaussian distribution with a mean value (standard deviation) for $\mathcal{R}^{\text{corr.},i}$ taken from the first (last) column of Table 4 of Ref. [15]. As a consistency check the average of the different mass values obtained is calculated. Its value agrees within 0.1 GeV with the value obtained using Eq. (14). The systematic uncertainties are estimated as the standard deviation of the individual fit results.

A full implementation of the systematic effects is thus missing in our study, however, we expect that the results given here represent a reasonable approximation. The theoretical uncertainties are evaluated by repeating the fit with different choices for the PDF and renormalization and factorization scales. The PDF uncertainty is taken as the maximum difference between the nominal result and the mass obtained with MSTW2008nlo90cl and NNPDF2.3 NLO. It has only a minor effect on the mass: $\Delta m_t(m_t) = 0.15$ GeV. The scale variation is determined as the asymmetric difference between the mass extracted with the central scale choice, $\mu = m_t(m_t)$, and with the scales $\mu_r$, $\mu_f$ set to $\mu_r = \mu_f = 2m_t(m_t)$ and $\mu_r = \mu_f = m_t(m_t)/2$. The two theory uncertainties are added in quadrature. For the determination of the aforementioned uncertainties, we used the theoretical $\mathcal{R}$ distribution calculated with $\mu = m_t(m_t) = 166$ GeV as pseudo data instead of $\mathcal{R}^{\text{corr.},i}$ as determined in Ref. [15] to avoid that statistical fluctuations of the experimental data introduces a bias in the evaluation of the theoretical uncertainties.

As a final result we obtain for the running top-quark mass:

$$m_t(m_t) = 165.9 \pm 1.4\ (\text{stat.}) \pm 1.3\ (\text{syst.})^{+1.5}_{-0.6}\ (\text{theory})\ \text{GeV},$$

where the central value and the statistical uncertainty are evaluated using Eq. (14) while the systematic and theoretical uncertainties are determined using Eq. (15) as described above. We have not included the uncertainty due to the parametric uncertainty of the QCD coupling constant because it has been shown in Ref. [15] that the impact is negligible. Comparing with Ref. [15], we observe a slight decrease of the experimental uncertainties. Combining the individual uncertainties in quadrature, we find

$$m_t(m_t) = 165.9^{+2.4}_{-2.0}\ (\text{total})\ \text{GeV}.$$

Comparing with the result for the top-quark pole mass as given in Ref. [15]

$$M_t^{\text{pole}} = 173.7 \pm 1.5\ (\text{stat.}) \pm 1.4\ (\text{syst.})^{+1.0}_{-0.5}(\text{theory})\ \text{GeV}\ [15],$$

we find that the theoretical uncertainties are larger in the extraction of $m_t(m_t)$. In both cases the theoretical uncertainty is largely dominated by the scale variation while the PDF effects give only a small contribution. Inspecting the individual bins it turns out that the bin closest to the threshold is responsible for the larger scale dependence when using the $\overline{\text{MS}}$ mass. Most likely this is due to the appearance of the derivative in Eq. (11), which can lead to a sizable contribution in the threshold region where $\mathrm{d}\sigma/\mathrm{d}m$ is large. Given the high sensitivity with respect to the top-quark mass this leads to an important contribution to the scale variation of the extracted mass value. We also note that with respect to the behavior of the perturbative expansion the two schemes, pole mass and running mass, are on an equal footing: as can be seen from Eq. (5) no large logarithms are involved in the relation between $M_t^{\text{pole}}$ and $m_t(m_t)$. The slight improvement of the scale dependence in the inclusive $t\bar{t}$ cross sections is to a large extent a kinematic effect, since the numerically smaller mass value in the running mass scheme increases the Born approximation and thus reduces the size of the corrections, leading to a somewhat smaller scale variation. As explained above, distributions may show a different behavior.

As a consistency check of the determination of the running mass one can convert the extracted mass value into the pole mass scheme and vice versa. Since in both cases the quality of the perturbative expansion is comparable we do not expect any major differences. The result of this exercise is shown in Table 2. Indeed the results are in perfect agreement with each other. Note that we included only the first non-trivial term in $\alpha_s$ in the conversion. This is a consistent approximation within the NLO accuracy presented here. Furthermore, no uncertainty due to the mass conversion itself is considered.

**Table 2** Top-quark mass extracted in the pole mass scheme and converted to the running mass scheme and vice versa

| Theory | $m_t(m_t)$ (GeV) | | $M_t^{\text{pole}}$ (GeV) |
|---|---|---|---|
| $\mathcal{R}(m_t(m_t))$ | $165.9^{+2.4}_{-2.0}$ | $\rightarrow$ | $173.5^{+2.5}_{-2.1}$ |
| $\mathcal{R}(M_t^{\text{pole}})$ | $165.8^{+2.2}_{-2.0}$ | $\leftarrow$ | $173.7^{+2.3}_{-2.1}$ |

## 4 Conclusion

In this article the NLO QCD corrections for top-quark pair production in association with an additional jet have been calculated defining the top-quark mass in the $\overline{\text{MS}}$ scheme instead of the top-quark pole mass commonly used. As a proof of concept, we have shown that it is possible to determine the top-quark running mass from the measurement of the differential cross section of $t\bar{t}$ + 1-jet production. Using the data from Ref. [15] we find

$$m_t(m_t) = 165.9 \pm 1.4\ (\text{stat.}) \\ \pm 1.3\ (\text{syst.})^{+1.5}_{-0.6}\ (\text{theory})\ \text{GeV},$$

which is – when translated to the pole mass scheme – consistent with the measurement of the pole mass. Since we extract the running top-quark mass at the scale of the top-quark mass itself, the conversion between the two mass schemes does not involve large logarithms. As a consequence, a major improvement concerning the convergence of the perturbative expansion is not expected. Using $m_t(m_t)$ is appropriate for the measurements reported in Ref. [15] which is based on 7 TeV data collected in run I. Due to the limited statistics, the moderate collider energy, and the large sensitivity of the bin closest to the threshold, high energetic events ($\rho_s < 0.4$) have only little impact on the analysis. Setting the renormalization scale equal to the top-quark mass and using $m_t(m_t)$ should thus provide reliable results. This is supported by the good agreement between the mass measurement using the pole mass and the mass measurement using the running mass. The larger theory uncertainty when using the running mass is due to the high mass sensitivity of the differential cross section close to the threshold and its larger scale dependence. As one can read off from Table 1 the scale variation of the sixth bin is roughly twice as large as the scale variation in bins three, four, and five. (The scale variation of bin one and two is similar or even larger than that of bin six, however, due to the small number of events (about 10% of the total number of events) and the reduced sensitivity, these two bins do not significantly affect the outcome of the analysis.)

We note that the measurement of the running mass gives an interesting and complementary description to that obtained with the pole mass. With more high energetic events available in run II it could also be interesting to determine $m_t(\mu)$ where the renormalization scale is set to some large value reflecting the typical momentum transfer in the considered $\rho_s$ bin (in the case that several bins are used). This would give the opportunity to 'measure' the running of the top-quark mass. Furthermore, at large scales the perturbative expansion using the running top-quark mass may be improved since the conversion introduces now potentially large logarithms which may cancel corresponding terms explicit in the calculation. However, given the significantly smaller sensitivity for low $\rho_s$ large statistics and a very good control of the systematic uncertainties would be required.

**Acknowledgements** We would like to thank T. Carli and F. Deliot for their careful reading of the manuscript and their valuable comments. This work is partially supported by the German Federal Ministry for Education and Research (Grant 05H15KHCAA), the Spanish Ministry of Economy, Industry and Competitiveness (MINEICO/FEDER-UE, FPA2015-65652-C4-3-R) and by the Marie Curie Initial Training Network of the European Union HiggsTools-ITN, No. 316704, FP7-PEOPLE-2012-ITN.



## Appendix

See Tables 3 and 4.

**Table 3** Same as Table 1 but for the NNPDF2.3 PDF set. Only the central scale $\mu = m_t(m_t)$ is shown

| Bin, range in $\rho_s$ | $\mathcal{R}(m_t(m_t))$ | | |
|---|---|---|---|
| | 160 GeV | 161 GeV | 162 GeV |
| 1, 0–0.25 | 0.115 | 0.117 | 0.118 |
| 2, 0.25–0.325 | 1.057 | 1.056 | 1.060 |
| 3, 0.325–0.425 | 1.918 | 1.940 | 1.968 |
| 4, 0.425–0.525 | 2.484 | 2.520 | 2.525 |
| 5, 0.525–0.675 | 2.163 | 2.151 | 2.157 |
| 6, 0.675–1.0 | 0.392 | 0.378 | 0.364 |

| Bin | 163 GeV | 164 GeV | 165 GeV | 166 GeV |
|---|---|---|---|---|
| 1 | 0.120 | 0.122 | 0.124 | 0.127 |
| 2 | 1.088 | 1.096 | 1.115 | 1.131 |
| 3 | 1.971 | 2.018 | 2.036 | 2.048 |
| 4 | 2.546 | 2.567 | 2.592 | 2.602 |
| 5 | 2.153 | 2.131 | 2.132 | 2.127 |
| 6 | 0.350 | 0.336 | 0.317 | 0.306 |

| Bin | 167 GeV | 168 GeV | 169 GeV | 170 GeV |
|---|---|---|---|---|
| 1 | 0.128 | 0.130 | 0.132 | 0.136 |
| 2 | 1.143 | 1.155 | 1.179 | 1.194 |
| 3 | 2.082 | 2.104 | 2.127 | 2.154 |
| 4 | 2.619 | 2.645 | 2.640 | 2.644 |
| 5 | 2.119 | 2.107 | 2.103 | 2.097 |
| 6 | 0.290 | 0.276 | 0.266 | 0.253 |

**Table 4** Same as Table 1 but for the MSTW2008nlo PDF set. Only the central scale $\mu = m_t(m_t)$ is shown

| Bin, range in $\rho_s$ | $\mathcal{R}(m_t(m_t))$ | | |
|---|---|---|---|
| | 160 GeV | 161 GeV | 162 GeV |
| 1, 0–0.25 | 0.119 | 0.120 | 0.124 |
| 2, 0.25–0.325 | 1.045 | 1.065 | 1.072 |
| 3, 0.325–0.425 | 1.919 | 1.926 | 1.968 |
| 4, 0.425–0.525 | 2.460 | 2.490 | 2.521 |
| 5, 0.525–0.675 | 2.163 | 2.156 | 2.144 |
| 6, 0.675–1.0 | 0.398 | 0.385 | 0.364 |

| Bin | 163 GeV | 164 GeV | 165 GeV | 166 GeV |
|---|---|---|---|---|
| 1 | 0.124 | 0.128 | 0.128 | 0.130 |
| 2 | 1.094 | 1.097 | 1.119 | 1.144 |
| 3 | 1.994 | 2.003 | 2.027 | 2.047 |
| 4 | 2.527 | 2.545 | 2.567 | 2.580 |
| 5 | 2.140 | 2.154 | 2.131 | 2.130 |
| 6 | 0.351 | 0.332 | 0.323 | 0.306 |

| Bin | 167 GeV | 168 GeV | 169 GeV | 170 GeV |
|---|---|---|---|---|
| 1 | 0.136 | 0.136 | 0.136 | 0.141 |
| 2 | 1.157 | 1.167 | 1.182 | 1.208 |
| 3 | 2.070 | 2.091 | 2.115 | 2.133 |
| 4 | 2.588 | 2.612 | 2.629 | 2.649 |
| 5 | 2.124 | 2.115 | 2.110 | 2.089 |
| 6 | 0.292 | 0.280 | 0.266 | 0.255 |

## References


1. CDF Collaboration, F. Abe et al., Observation of top quark production in $\bar{p}p$ collisions. Phys. Rev. Lett. **74**, 2626–2631 (1995). arXiv:hep-ex/9503002
2. D0 Collaboration, S. Abachi et al., Observation of the top quark. Phys. Rev. Lett. **74**, 2632–2637 (1995). arXiv:hep-ex/9503003
3. ATLAS, CDF, CMS, D0 Collaboration, First combination of Tevatron and LHC measurements of the top-quark mass. arXiv:1403.4427 [hep-ex]
4. G. Degrassi, S. Di Vita, J. Elias-Miro, J.R. Espinosa, G.F. Giudice et al., Higgs mass and vacuum stability in the Standard Model at NNLO. JHEP **1208**, 098 (2012). arXiv:1205.6497 [hep-ph]
5. S. Alekhin, A. Djouadi, S. Moch, The top quark and Higgs boson masses and the stability of the electroweak vacuum. Phys. Lett. B **716**, 214–219 (2012). arXiv:1207.0980 [hep-ph]
6. G. Cortiana, Top-quark mass measurements: review and perspectives. Rev. Phys. **1**, 60–76 (2016). arXiv:1510.04483 [hep-ex]
7. ATLAS, CMS Collaboration, M. Vos, Top-quark mass measurements at the LHC: alternative methods. PoS TOP2015, 035 (2016). arXiv:1602.00428 [hep-ex]
8. A.H. Hoang et al., Top–anti-top pair production close to threshold: synopsis of recent NNLO results. Eur. Phys. J. Direct **C3**, 1–22 (2000). arXiv:hep-ph/0001286
9. I.I.Y. Bigi, M.A. Shifman, N.G. Uraltsev, A.I. Vainshtein, The Pole mass of the heavy quark. Perturbation theory and beyond. Phys. Rev. D **50**, 2234–2246 (1994). arXiv:hep-ph/9402360
10. M. Beneke, V.M. Braun, Heavy quark effective theory beyond perturbation theory: renormalons, the pole mass and the residual mass term. Nucl. Phys. B **426**, 301–343 (1994). arXiv:hep-ph/9402364
11. M. Beneke, P. Marquard, P. Nason, M. Steinhauser, On the ultimate uncertainty of the top quark pole mass. arXiv:1605.03609 [hep-ph]
12. U. Langenfeld, S. Moch, P. Uwer, Measuring the running top-quark mass. Phys. Rev. D **80**, 054009 (2009). arXiv:0906.5273 [hep-ph]
13. S. Alekhin, S. Moch, S. Thier, Determination of the top-quark mass from hadro-production of single top-quarks. arXiv:1608.05212 [hep-ph]
14. S. Alioli, P. Fernandez, J. Fuster, A. Irles, S.-O. Moch, P. Uwer, M. Vos, A new observable to measure the top-quark mass at hadron colliders. Eur. Phys. J. C **73**, 2438 (2013). arXiv:1303.6415 [hep-ph]
15. ATLAS Collaboration, Determination of the top-quark pole mass using $t\bar{t}$ + 1-jet events collected with the ATLAS experiment in 7 TeV pp collisions. JHEP **10**, 121 (2015). arXiv:1507.01769 [hep-ex]
16. CMS Collaboration, Determination of the normalised invariant mass distribution of $\mathrm{t\bar{t}}$+jet and extraction of the top quark mass, CMS-PAS-TOP-13-006
17. S. Dittmaier, P. Uwer, S. Weinzierl, NLO QCD corrections to t anti-t + jet production at hadron colliders. Phys. Rev. Lett. **98**, 262002 (2007). arXiv:hep-ph/0703120
18. S. Dittmaier, P. Uwer, S. Weinzierl, Hadronic top-quark pair production in association with a hard jet at next-to-leading order QCD: Phenomenological studies for the Tevatron and the LHC. Eur. Phys. J. C **59**, 625–646 (2009). arXiv:0810.0452 [hep-ph]
19. K. Melnikov, M. Schulze, NLO QCD corrections to top quark pair production and decay at hadron colliders. JHEP **08**, 049 (2009). arXiv:0907.3090 [hep-ph]
20. K. Melnikov, M. Schulze, NLO QCD corrections to top quark pair production in association with one hard jet at hadron colliders. Nucl. Phys. B **840**, 129–159 (2010). arXiv:1004.3284 [hep-ph]
21. M. Cacciari, G.P. Salam, G. Soyez, The anti-k(t) jet clustering algorithm. JHEP **0804**, 063 (2008). arXiv:0802.1189 [hep-ph]
22. M. Cacciari, G.P. Salam, G. Soyez, FastJet user manual. Eur. Phys. J. C **72**, 1896 (2012). arXiv:1111.6097 [hep-ph]
23. P.M. Nadolsky et al., Implications of CTEQ global analysis for collider observables. Phys. Rev. D **78**, 013004 (2008). arXiv:0802.0007 [hep-ph]
24. A. Martin, W. Stirling, R. Thorne, G. Watt, Parton distributions for the LHC. Eur. Phys. J. C **63**, 189–285 (2009). arXiv:0901.0002 [hep-ph]
25. R.D. Ball et al., Parton distributions with LHC data. Nucl. Phys. B **867**, 244–289 (2013). arXiv:1207.1303 [hep-ph]
26. G. Bevilacqua, H.B. Hartanto, M. Kraus, M. Worek, Top quark pair production in association with a jet with next-to-leading-order QCD off-shell effects at the large hadron collider. Phys. Rev. Lett. **116**(5), 052003 (2016). arXiv:1509.09242 [hep-ph]
27. G. Bevilacqua, H.B. Hartanto, M. Kraus, M. Worek, Off-shell top quarks with one jet at the lhc: a comprehensive analysis at NLO QCD. JHEP **11**, 098 (2016). arXiv:1609.01659 [hep-ph]
28. T. Jeo, P. Nason, On the treatment of resonances in next-to-leading order calculations matched to a parton shower. JHEP **12**, 065 (2015). arXiv:1509.09071 [hep-ph]
29. T. Jeo, J.M. Lindert, P. Nason, C. Oleari, S. Pozzorini, An NLO+PS generator for $t\bar{t}$ and $Wt$ production and decay including non-resonant and interference effects. Eur. Phys. J. C **76**(12), 691 (2016). arXiv:1607.04538 [hep-ph]
30. K. Hagiwara, Y. Sumino, H. Yokoya, Bound-state effects on top quark production at hadron colliders. Phys. Lett. B **666**, 71–76 (2008). arXiv:0804.1014 [hep-ph]
31. Y. Kiyo, J.H. Kuhn, S. Moch, M. Steinhauser, P. Uwer, Top-quark pair production near threshold at LHC. Eur. Phys. J. C **60**, 375–386 (2009). arXiv:0812.0919 [hep-ph]